Spectroscopic Evidence for Nanosecond Protein Relaxation after Photodissociation of Myoglobin−CO[†]

Raymond M. Esquerra, Robert A. Goldbeck,* Daniel B. Kim-Shapiro,[‡] and David S. Kliger

Department of Chemistry and Biochemistry, University of California at Santa Cruz, Santa Cruz, California 95064

Received June 17, 1998; Revised Manuscript Received October 15, 1998

ABSTRACT: Nanosecond time-resolved absorption and magnetic optical rotatory dispersion (MORD) measurements of photolyzed myoglobin−CO visible bands (500−650 nm) are presented. These measurements reveal a 400 ns process, spectrally distinct from ligand recombination, that accounts for 7% of the observed spectral evolution in the visible absorption bands and 4% in the MORD. The time-resolved MORD, more sensitive to heme coordination geometry than absorption, suggests that this process is most likely associated with protein relaxation on the distal side of the heme pocket, perhaps accompanying rehydration of the deoxymyoglobin photoproduct or accommodation of protein side chains to ligand escape.

Myoglobin (Mb)[1] is a monomeric protein that transports O_2 from hemoglobin to the terminal mitochondrial oxidase in muscle by reversibly binding molecular oxygen at an embedded heme covalently attached to the protein at the proximal histidine, His93. Mb has an affinity for oxygen nearly 100 times larger than that of model heme compounds (*1*). Conversely, the protein has a substantially reduced affinity for carbon monoxide compared with free heme. The ratio of the binding affinities, K_{CO}/K_{O_2}, is ∼20000 for simple protoheme complexes in benzene compared with ∼20 for Mb (*2*). This differentiation of ligands allows myoglobin to act as a biological oxygen transport protein in the presence of minute levels of exogenous and endogenous CO, the latter resulting from heme catabolism and cellular signaling (*3*−*5*). Because the binding affinity of ligands differs in free heme and model compounds relative to those of heme proteins, the protein matrix must affect ligand binding and does not simply serve as a hydrophobic pocket to protect the heme from autoxidation.

In the past decade, X-ray structures of myoglobin site-directed mutants, combined with kinetic and equilibrium ligand binding measurements, have provided insight into the nature of ligand binding in myoglobin (for reviews, see refs *6* and *7*). In particular, mutant studies have shown that electrostatic interaction between the distal histidine, His64, and the bound ligand serves to distinguish myoglobin affinity for O_2, NO, and CO from the ligand affinities of simple protoheme models (*2*, *7*). Steric interactions between His64 and the bound ligand were traditionally thought to increase the energy of the CO-bound complex by preventing an energetically preferred linear binding geometry (*3*, *8*). However, studies of myoglobin mutants indicate that steric interference by His64 with ligand binding plays only a minor role in differentiating the affinities for CO and O_2, and most of the discrimination arises from electrostatic interactions between His64 and the bound ligand (*6*, *7*).

X-ray crystallography reveals a water molecule in the pocket of WT SW deoxyMb that is hydrogen bonded to the N_ϵ of His64 with about 80% occupancy (Figure 1). This water must be removed from the pocket before a ligand can bind to the distal side of the heme, as X-ray structures of CO-ligated myoglobin show a lack of hydration (*1*). The water inhibits the binding of both CO and O_2 compared to model heme complexes in organic solvents (*6*). Conversely, because the Fe−(O−O) complex is highly polar, hydrogen bonding to N_ϵ of His64 stabilizes oxymyoglobin by at least ∼2 kcal/mol (*9*). Since it forms a less polar bond with the heme iron of Mb, any favorable interactions between the bound CO and His64 are thought to be weak compared to those for oxygen. These mechanisms are supported by general trends in myoglobin mutants in which His64 was substituted with apolar residues. Apolar substitutions with a dehydrated pocket (*1*) yield an increase in binding rates for both CO and O_2 due to the removal of the hydrogen-bonded water molecule, but a dramatic decrease in the affinity of O_2 (*2*, *6*, *7*) resulting from the loss of favorable electrostatic interactions. Although the rate of CO association is limited by bond formation, the displacement of the distal water molecules affects the overall rate constant by modifying the equilibrium between CO in the distal pocket and the final binding site (*6*, *10*−*12*). For oxygen, the distal water effects the binding by obstructing access to the heme pocket by the O_2 ligand (*6*).

X-ray structures also reveal that there is no major pathway for ligands to reach the heme binding site, so there must be dynamical fluctuations that enable ligand entry and escape between the heme and the solvent (*13*). It is desirable to determine which, if any, kinetic barriers exist to ligand entry and escape and what protein conformational changes are associated with these barriers to understand ligand binding

[†] Supported by NIH Grant GM38549.

* To whom correspondence should be addressed.

[‡] Present address: Department of Physics, Wake Forest University, Winston-Salem, NC 27109-7507.

[1] Abbreviations: MORD, magnetic optical rotatory dispersion; MCD, magnetic circular dichroism; TROA, time-resolved optical absorption; TRMORD, time-resolved MORD; Mb, myoglobin; HMb, human myoglobin; Hb, hemoglobin; WT, wild type; SW, sperm whale; SVD, singular value decomposition.

10.1021/bi9814437 CCC: $15.00
Published on Web 11/19/1998

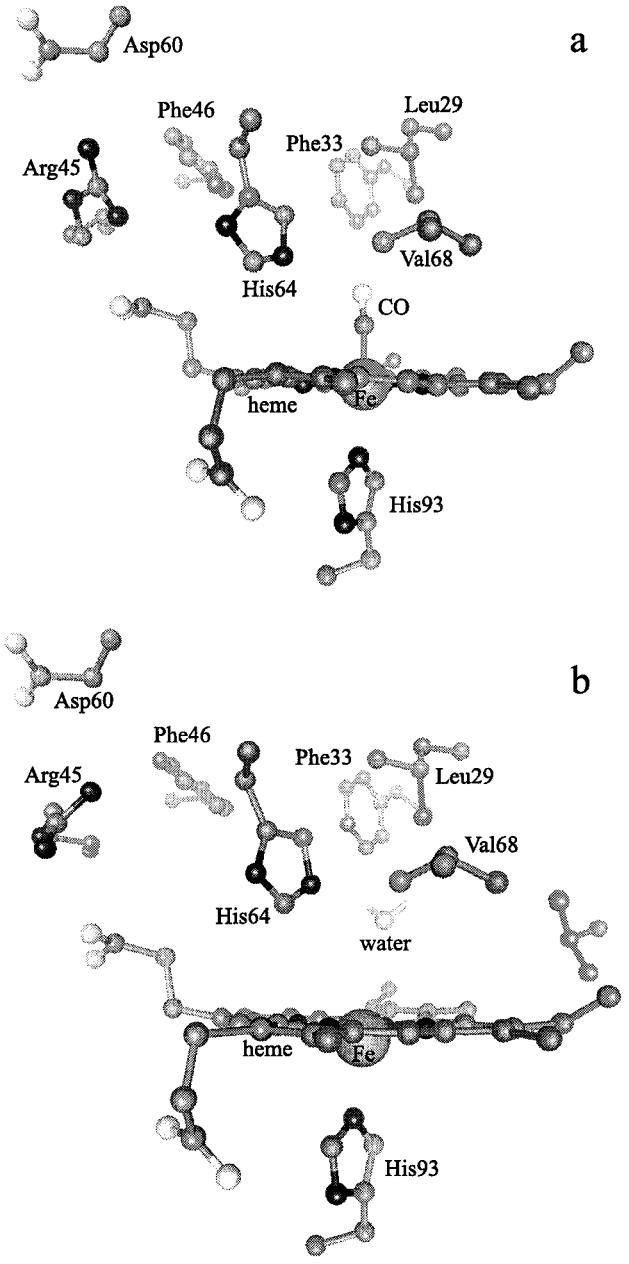

FIGURE 1: Side views of the distal pocket in SW (a) carbonmonoxy- and (b) deoxymyoglobin crystal structures, shown in perspective with lighter shading indicating distance. Residues are shown with carbon (and iron) atoms in gray, oxygen atoms in white, and nitrogen atoms in black. Hydrogen atoms on the distal pocket water molecule are shown as sticks. Structures for panels a and b were taken from Brookhaven Protein Data Bank files 2mgk and 2mgl, respectively (*63*).

regulation in biological heme proteins such as myoglobin. Mutations of other distal residues in SW Mb have provided insights into the protein's role in ligand binding (*1*, *6*) and a better understanding of the role of distal residues.

In addition to the mutations of sperm whale myoglobin described above, human myoglobin (HMb) has been the focus of many mutation studies (*14*−*18*). These studies also show a complicated relationship between the binding of ligands and the nature of the substituted residues. Time-resolved absorption studies in the Soret band of HMb and site-specific mutants of HMb reveal a microsecond process that is attributed to protein relaxations allowing the escape of ligand from the protein matrix to the solvent (*15*−*17*).

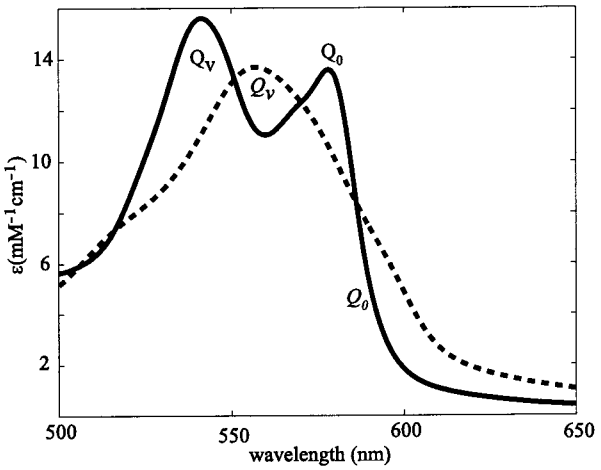

FIGURE 2: Visible (Q) band absorption spectra of MbCO (—) and deoxyMb (---). Q_v and Q_0 denote vibronic and vibration-less transitions for MbCO, respectively. Italicized Q_v and Q_0 denote Mb transitions.

These relaxations were explained by the X-ray structure of HMb, which shows a salt bridge between Lys45 (Arg in SW Mb), Asp60, and a heme propionate (*15*, *17*). Further mutagenic studies (*14*, *16*, *18*) of HMb showed that this salt bridge does not influence the rate-determining step, and a more complicated picture of residue motion is needed to explain the control of ligand association and dissociation.

Most time-resolved absorption studies of myoglobin have focused on the Soret band (380−460 nm), but the visible, or Q, bands (480−650 nm) can provide additional information. The Q bands consist of two bands, the Q(0,0) (Q or Q_α) and Q(1,0) (Q_v or Q_β) bands, corresponding to transitions to the origin and to the first vibrationally excited level, respectively, of the lowest excited electronic state (*19*, *20*). In low-spin ferrous hemes (e.g., MbCO), these transitions are separated and have relative intensities and energies that vary with ligand species. In high-spin five-coordinate ferrous hemes (Mb), the Q_o appears as a small shoulder on the more dominant Q_v transition (*20*−*23*). Figures 2 and 3 give the equilibrium absorption, MORD, and ORD spectra of Mb and MbCO in the visible bands. Although the one-electron orbital transitions associated with the visible bands are forbidden by symmetry in a simple non-interacting-electron ring model of conjugated π-systems, a model which includes interactions between electrons breaks this symmetry restriction and mixes these transitions with the strongly allowed transition associated with the Soret bands (*19*). This mixing is called configuration interaction (CI), and the Q bands can be said to borrow intensity from the Soret band via this mechanism (*19*−*21*), in analogy to the intensity borrowing that is often associated with vibronic coupling between weakly and strongly allowed transitions in polyatomic molecules. Moreover, the relative intensity of vibronic transitions compared to that of the vibration-less electronic transition for the Q bands is much larger than in the Soret band (*21*−*23*), making the vibrational structure of the Q bands more sensitive to heme changes which affect vibronic coupling than the Soret band. Hence, spectroscopic studies of the electronic origin and vibronic transitions of the visible bands may provide information about protein dynamics not available from Soret band studies.

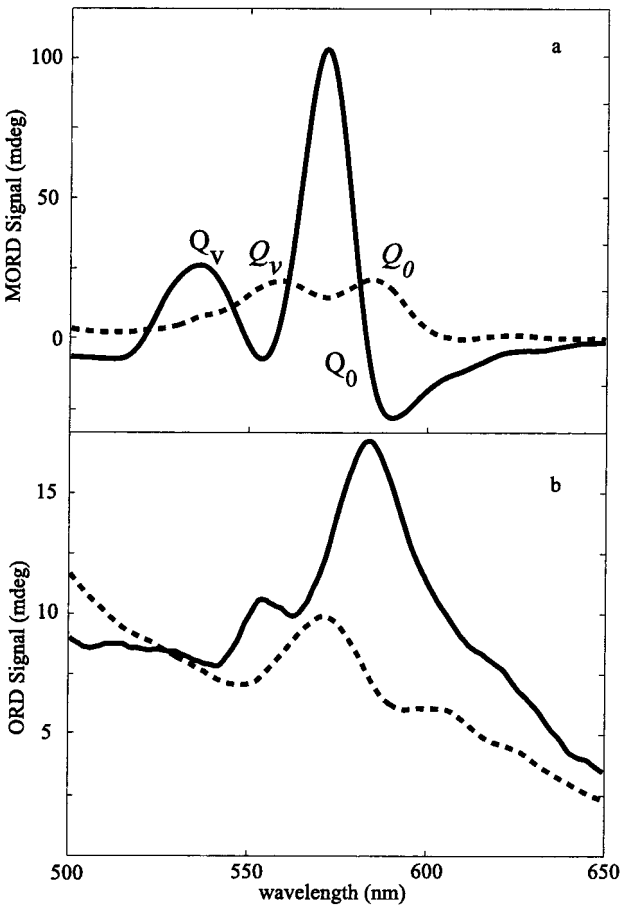

FIGURE 3: MORD and ORD spectra for MbCO (—) and Mb (---) measured on the near-null MORD instrument with a sample concentration of 120 μM, a path length of 5 mm, and a field strength of 1 T: (a) MORD and (b) ORD.

The nanosecond time-resolved visible band magnetic optical rotatory dispersion and absorption measurements presented here show spectral changes occurring in hundreds of nanoseconds after photolysis that are not characteristic of ligand recombination. We discuss these changes in terms of the protein structural changes that occur as photolyzed myoglobin relaxes to equilibrium deoxyMb.

MATERIALS AND METHODS

Time-Resolved Natural and Magnetic Optical Rotatory Dispersion Measurements. Magnetic optical activity results from the chirality induced in a chromophore by a magnetic field and is sensitive to environmental perturbations of chromophore electronic energies, in contrast to natural optical activity, which arises from the inherent chirality of the chromophore structure or environment. Magnetic optical activity has proven to be a particularly valuable tool in understanding coordination geometry and its relationship to the protein environment near the heme chromophore in heme proteins (*24*−*26*). Magnetic optical activity consists of an absorptive part, magnetic circular dichroism (MCD), and a dispersive part, magnetic optical rotatory dispersion (MORD). The absorptive and dispersive parts, being the imaginary and real parts, respectively, of a complex index of refraction for circularly polarized light, are related by the Kramers−Kronig transforms (*27*, *28*). [Magnetic optical rotation is also known as the Faraday effect (*28*).] With the advent of modern circular dichroism instrumentation based on photoelastic modulators and phase sensitive detection, the use of MCD has eclipsed MORD as a probe of the magnetic optical activity of chromophores. In principle, however, they contain identical information (*29*). In practice, they may be interconverted with reasonable accuracy using approximate Kramers−Kronig transforms that are limited to particular absorption bands when these are well separated from neighboring bands, such as the visible bands in porphyrins and heme proteins being separated from the higher-energy Soret transitions. The general transforms are

$$\mathrm{MORD}(\nu) = \frac{\nu^2}{\pi}\int_0^\infty \frac{\mathrm{MCD}(\nu')}{\nu'(\nu'^2 - \nu^2)}\mathrm{d}\nu' \quad (1)$$

$$\mathrm{MCD}(\nu) = \frac{-4\nu^3}{\pi}\int_0^\infty \frac{\mathrm{MORD}(\nu')}{\nu'^2(\nu'^2 - \nu^2)}\mathrm{d}\nu' \quad (2)$$

Although the integrals in eqs 1 and 2 run over all frequencies, we limited the transform calculations to frequencies within the visible bands (500−650 nm). We previously found that such an approximate transform procedure worked well for the natural Soret CD and ORD of hemoglobin (*30*).

As magnetic and natural optical activity are sensitive to complementary aspects of protein structure (*24*−*26*, *31*−*33*), time-resolved measurements of both properties in biological chromophores are useful in understanding the structural changes that occur while proteins perform their biological functions. To this end, we have developed methods for measuring nanosecond time-resolved optical rotatory dispersion spectra, both natural and magnetic (*30*, *34*−*35*). The basic optical principle of the TRORD and TRMORD techniques is a near-null polarimetric method, first described by Keston and Lospalluto (*36*). A full derivation of the optical basis of the TRMORD technique and an investigation of possible artifacts and their amelioration, particularly those associated with photoselection-induced ordering of the sample, have been presented elsewhere (*34*, *35*, *37*). Briefly, a MORD measurement is made by placing a sample between two crossed polarizers and then rotating one polarizer, first clockwise (facing the probe source) and then counterclockwise, by a small angle, β, from the crossed position. (The effect of any Faraday rotation contributed by the solvent and cell windows is canceled from multichannel measurements of the sample's MORD by an additional optical device, a Faraday compensator, placed between the polarizers.) The signal is defined as the difference of the detected intensities for the clockwise and counterclockwise positions, normalized to their sum,

$$s_\mathrm{D}(t) = \frac{I_{+\beta}(t) - I_{-\beta}(t)}{I_{+\beta}(t) + I_{-\beta}(t)} \quad (3)$$

where the subscript D denotes the direction of the magnetic field, parallel (P) or antiparallel (A) with respect to the probe propagation direction. Using the small angle approximation, the intensity transmitted through crossed polarizers is proportional to the square of the total rotation, (HMORD ±

$\beta)^2$, for a parallel field of strength H. Thus

$$s_p(t) = \frac{-2\beta H\text{MORD}}{\beta^2 + H^2\text{MORD}} \cong \frac{-2H\text{MORD}}{\beta} \quad (4)$$

when $H\text{MORD} \ll \beta$.

Sample Preparation and Data Collection. Myoglobin from horse skeletal muscle (Sigma) was diluted with 0.1 mM sodium phosphate buffer (pH 7.3) to give a final concentration of about 120 μM. The sample was reduced with excess sodium dithionite (1 mM) and anaerobically sealed under 1 atm of CO in a 5 mm path length S1-UV quartz cell. The time-resolved optical absorption (TROA) measurements (128 scans) were taken at 62 different times, spaced logarithmically (ten per decade) from 25 ns to 10 ms after laser photolysis, using a 16 ns detector gate. The TRMORD (TRORD) measurements (2048 scans) were taken using a 150 ns detector gate at 45 different delay times (eight per decade) ranging from 90 ns to 10 ms after laser photolysis. The laser timing was defined relative to the center of the detector gate. The sample temperature was 26 °C. Equilibrium absorption measurements were taken on a Shimadzu UV-2101 spectrophotometer with a 1 nm bandwidth and a 0.2 nm sampling interval. Absorption spectra taken before and after the photolysis experiments were indistinguishable, indicating that there was no significant sample decomposition.

Instrumentation. The time-resolved absorption measurements were performed with the instrumentation described previously (*38*, *39*). A xenon flash lamp produced unpolarized white light that was collimated (8 mm diameter) through the sample. It was then focused through a 250 μm slit into a Jarrel Ash spectrograph (150 grooves/mm, 800 nm blaze grating) and detected with an EG&G OMA II detector. A Stanford Instruments DG535 delay/pulse generator controlled the timing of the detector gate and the firing of the flash lamp with respect to the laser pulse. A frequency-doubled (532 nm) Quanta Ray DCR-2A Nd:YAG laser produced 8 ns excitation pulses at 2 Hz (10 mm diameter). The pulse energy was 40 mJ/pulse. The excitation beam was polarized vertically by a Glan-laser polarizer and propagated at 90° with respect to the probe propagation direction. A second Glan-laser polarizer was placed in the path of the probe beam before the sample at magic angle, 54.7°, with respect to the polarization axis of the laser polarizer. Magic angle polarization of the probe beam minimizes any distortion of the observed kinetics due to artifacts associated with photoselection and rotational diffusion (*43*).

The TRMORD instrument was the same as the time-resolved absorption instrument except for the addition of a matched pair of electric dipole magnets (GMW Associates, model 3470, Redwood City, CA) and a second polarizer. The sample was placed between the crossed polarizers and magnetized parallel to the probe propagation direction with a field of 1 T. A solvent blank magnetized in an opposite field of equal strength served as the Faraday compensator, which distinguishes the rotation of the probe light polarization vector due to the sample from that due to the Faraday effect (*28*) of the solvent and cell window. A β value of 1.26° was used as the small reference rotation angle in the near-null polarimetric measurements (see eq 4). The 532 nm actinic beam energy was approximately 40 mJ/pulse at 2 Hz (10 mm diameter). After passing through the first polarizer, the probe light passes through the poles of the magnet (12 mm gap), entering both the sample and the compensator with a beam diameter of about 7 mm. A third polarizer was used to ensure horizontal polarization of the pump beam. The orientations of the probe polarizers before and after the sample were horizontal and vertical, respectively. The probe and pump propagation vectors were perpendicular. This crossed-excitation geometry eliminates photoselection-induced linear birefringence and dichroism contributions to the signal (*34*, *35*, *37*).

Analysis. Each time-resolved spectral scan, comprising 250 wavelength points between 500 and 650 nm, was smoothed using a 15-point Savitzky−Golay algorithm. The smoothed data were placed in an $n \times m$ matrix, $\mathbf{A}(\lambda,t)$, where n is the number of wavelengths and m is number of time points, and decomposed using the method of singular value decomposition (SVD) (*40*, *41*) into three matrixes,

$$\mathbf{A}(\lambda,t) = \mathbf{U}(\lambda)\mathbf{S}\mathbf{V}^{\mathrm{T}}(t) \quad (5)$$

where $\mathbf{U}$ is an $n \times m$ matrix ($n \geq m$) containing m orthogonal basis spectra as columns, $\mathbf{V}^{\mathrm{T}}$ is an $m \times m$ matrix that is the transpose of $\mathbf{V}$, each column of $\mathbf{V}$ giving the amplitude of the corresponding column of $\mathbf{U}$ at each time point, and $\mathbf{S}$ is an $m \times m$ diagonal matrix containing the singular values of $\mathbf{A}$, which weight the contributions of $\mathbf{U}$ and $\mathbf{V}$. In this decomposition, important spectral evolutions are associated with the largest singular values whereas the singular values associated with noise are usually found to fall below a well-defined cutoff value (*41*−*43*). If the number of significant values above this cutoff is s, then the truncated and noise-filtered data matrix, $\mathbf{A}_s$, is constructed from the matrix product of the first s columns of $\mathbf{U}$, the $s \times s$ subset of $\mathbf{S}$, and the first s rows of $\mathbf{A}^{\mathrm{T}}$. This is the best least-squares representation of $\mathbf{A}$, where the sum of squares difference between $\mathbf{A}$ and $\mathbf{A}_s$ is given by summing the squares of the discarded singular values (*41*).

The SVD-filtered data matrix was fit to a sum of exponentials using a nonlinear least-squares simplex fitting procedure as a means to give a model-independent examination of the data (*41*−*43*). The set of wavelength-dependent amplitudes associated with each exponential time constant is called a b-spectrum. The root sum of squares of each b-spectrum, normalized to the total for all the spectra, was used to measure the relative contribution of each b-spectrum to the overall spectral evolution, i.e., its (relative) amplitude.

RESULTS

Time-Resolved Optical Absorption (TROA). Figure 4 shows the TROA difference (transient minus prephotolysis) spectra of the Q band of myoglobin after CO photodissociation (85% net photolysis yield). The basis spectra and time courses for the largest three singular values of the data are shown in Figure 5. The first basis spectrum, $\mathbf{U}_1\mathbf{S}_1$, is the best one-component least-squares fit to the phototransformed MbCO (*41*), and $\mathbf{V}_1$ corresponds to the time evolution of this spectrum. As ligand rebinding is responsible for most of the spectral changes in this MbCO photolysis experiment, this basis spectrum and its time evolution are associated primarily with CO recombination. As expected, the $\mathbf{U}_1\mathbf{S}_1$ spectrum closely resembles a deoxyMb minus MbCO dif-

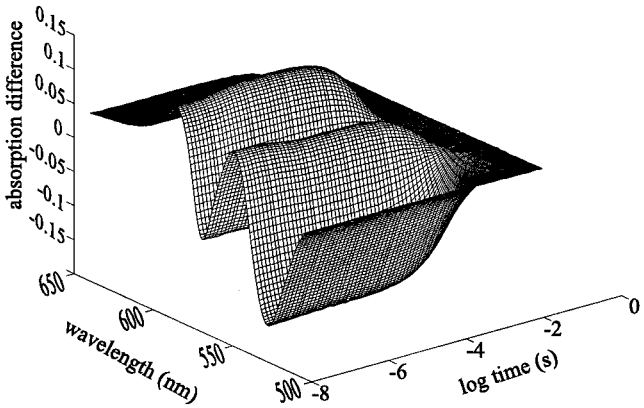

FIGURE 4: Three-dimensional plot of TROA difference spectra (transient minus prephotolysis) at 62 logarithmic times (ten per decade) from 25 ns to 10 ms after laser photolysis.

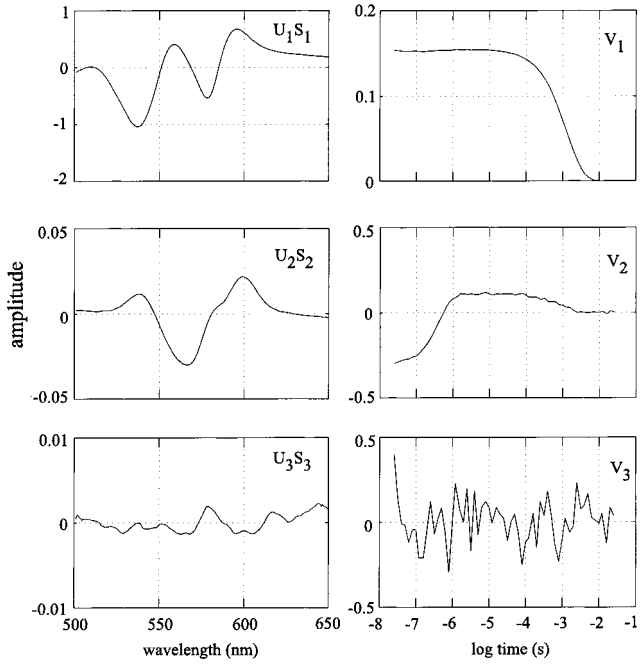

FIGURE 5: First three SVD basis spectra, **U**·**S** (left panels), and time amplitudes, **V** (right panels), for the data depicted in Figure 4.

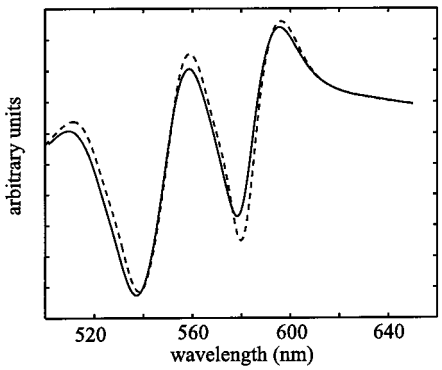

FIGURE 6: The band shape of the first SVD basis spectrum, $\mathbf{U}_1$ (—), is similar to that of the equilibrium deoxyMb minus MbCO difference spectrum (---).

ference spectrum, as shown in Figure 6. The second basis spectrum, $\mathbf{U}_2\mathbf{S}_2$, has a magnitude of about 5% of that of $\mathbf{U}_1\mathbf{S}_1$ and is very different from a deoxyCO difference spectrum. The corresponding time vector, $\mathbf{V}_2$, reflects an increasing contribution from this SVD component within the first microsecond, which remains relatively constant for about 100 μs and then decays with a lifetime of about 1 ms. The third basis spectrum, $\mathbf{U}_3\mathbf{S}_3$, appears to contain some real spectral features; however, its magnitude is less than 0.5% of the first basis spectrum, and its time course, $\mathbf{V}_3$, appears to be nearly random. The higher-order basis spectra are smaller in magnitude and contain no recognizable spectral or kinetic information. The matrix products of the first three basis spectra with their corresponding time courses were thus used as a truncated SVD representation of the time-resolved optical density measurements.

Table 1: Exponential Decay Time Constants and Amplitudes from Kinetic Analysis of MbCO TROA, TRMORD, and TRORD

	process 1		process 2	
method	τ_1 (ns)	amp_1	τ_2 (ms)	amp_2
TROA	370 ± 30	6.5 ± 0.2	1.3 ± 0.04	94.0 ± 0.1
TRORD[a]	—	—	1.0 ± 0.2	93 ± 1
TRMORD	580 ± 330	3.6 ± 1.5	1.2 ± 0.1	96 ± 1

[a] One-exponential fit.

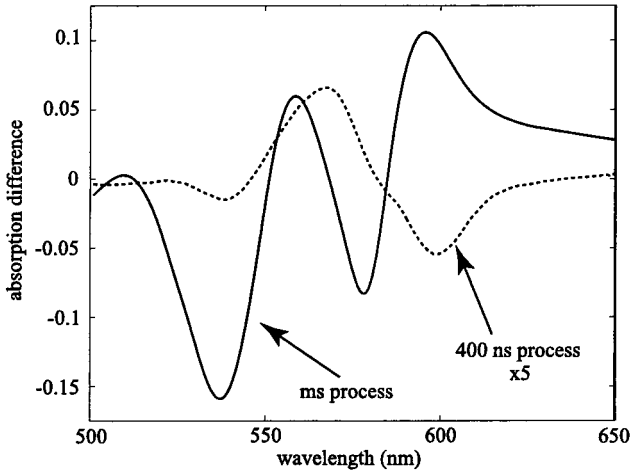

FIGURE 7: b-Spectra from a two-exponential fit of the time-resolved absorption data. (Note that the 300−400 ns process is multiplied by 5.) The dissimilarity of the spectra indicates that the first process is not entirely due to ligand rebinding.

A global kinetic fit of the SVD-filtered data to a sum of exponential decays reliably produced two time constants: τ_1 = 370 ns and τ_2 = 1.3 ms (Table 1). The corresponding b-spectra are shown in Figure 7. The b-spectrum for the millisecond process (τ_2) closely resembles the optical changes expected for bimolecular recombination of CO. The b-spectrum for τ_1, on the other hand, is clearly distinct from that expected for ligand recombination and measures protein relaxation after photolysis. This spectral change appears to correspond to a small blue shift and loss of intensity of the 560 nm deoxyMb band in combination with a growing in of a shoulder or broadening at about 600 nm. [We also tried modeling the first process with a stretched exponential, $e^{-(t/\tau)^a}$, sometimes used to represent relaxation from a distribution of conformational states. We found that this did not effect the shape of the spectral change or significantly change the rate or amplitude of this process compared with the simple exponential model.] Fits of the data to three exponentials led to less reproducible analyses and were thus determined to be unwarranted.

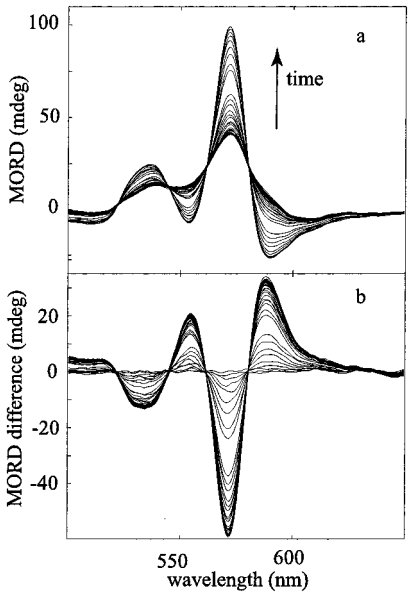

FIGURE 8: TRMORD spectra at 45 logarithmically spaced delay times (eight per decade) from 90 ns to 10 ms after ligand photolysis: (a) TRMORD and (b) difference TRMORD.

Time-Resolved Magnetic and Natural Optical Rotatory Dispersion. As both sensitivity and interpretability with respect to the heme environment are greater for magnetic optical activity than for absorption, further insight into the dynamics of photolyzed myoglobin can be gained from TRMORD measurements. MbCO complexes ($S = 0$) exhibit MCD spectra with simple A terms arising from porphyrin D_{4h} ($x-y$ degenerate) $\pi-\pi^*$ transitions, similar to the spectra of metalloporphyrins. High-spin ferrous ($S = 2$) deoxymyoglobin shows both A and C terms in the visible bands. The C terms are of particular interest because they arise from spin−orbit coupling with the iron and are sensitive to iron coordination chemistry. The corresponding MORD spectra comprise the Kramers−Kronig transforms of these A and C terms.

The TRMORD spectra and the difference spectra obtained at delay times from 90 ns to 10 ms are shown in Figure 8. The data were baseline offset in regions where the signal was near zero (710−750 nm). The offsets applied were less than 4% of the absolute signal. The basis vectors and the time courses of the time-resolved difference MORD spectra are shown in Figure 9. As was the case for absorption, the first basis spectrum ($\mathbf{U}_1\mathbf{S}_1$) resembles a deoxyMb minus MbCO difference spectrum and its time course ($\mathbf{V}_1$) decays in milliseconds. The magnitude of the second basis vector ($\mathbf{U}_2\mathbf{S}_2$) is a few percent of that of the first basis spectrum. $\mathbf{U}_2\mathbf{S}_2$ does not entirely resemble a deoxy minus CO difference spectrum, but rather contains information about the protein dynamics around the heme that appear as spectral changes in the MORD of photolyzed deoxyMb. The time course of this second basis spectrum rises to a constant level in about 500 ns and falls to zero in about 1 ms. Although some higher-order basis spectra such as $\mathbf{U}_3\mathbf{S}_3$ have spectral features, their magnitudes are smaller than that of $\mathbf{U}_2\mathbf{S}_2$, and their time courses seem random.

Global kinetic analyses of the SVD-filtered TRMORD and TRORD (data not shown) spectra are summarized in Table 1. As expected from the TROA results, process 2 closely resembles the equilibrium deoxyMb minus MbCO difference spectrum in MORD (Figure 10a) and MCD (Figure 10b). Process 1 has a lifetime of 500 ns and an amplitude of about 4% in the TRMORD data, with spectral features that distinguish it from the deoxy minus CO difference spectrum characterizing process 2. As expected from the equilibrium spectra (Figure 3), the absolute and photolysis difference TRORD spectra are much smaller in magnitude than the corresponding TRMORD spectra and thus have lower signal-to-noise values. Only the time course associated with the first singular value appears to be nonrandom. Global analysis yields only the millisecond bimolecular rebinding process seen in the TRMORD and TROA analyses. The relative

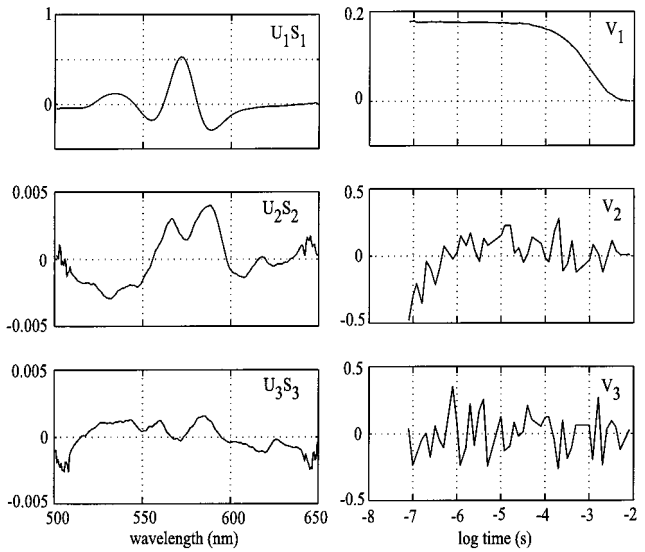

FIGURE 9: First three SVD basis spectra, $\mathbf{U}\cdot\mathbf{S}$ (left panels), and time amplitudes, $\mathbf{V}$ (right panels), for the difference TRMORD data depicted in Figure 8.

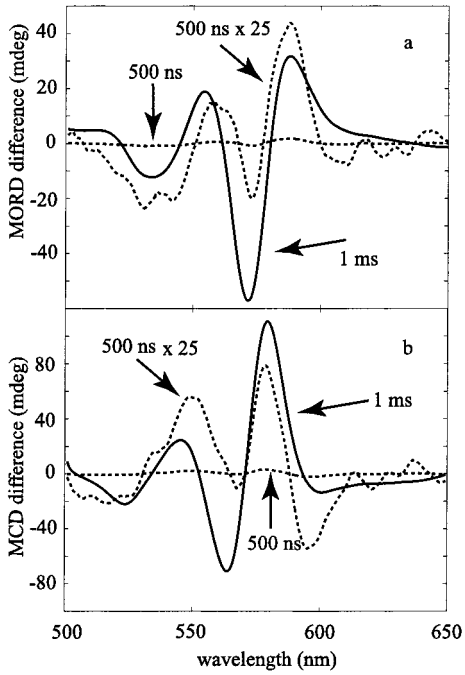

FIGURE 10: b-Spectra from a two-exponential fit to the TRMORD difference spectra: process 1, 500 ns (---); and process 2, 1 ms (—). (The 500 ns b-spectrum multiplied by 25 is shown for easier comparison.) (a) TRMORD difference b-spectra. (b) TRMCD difference b-spectra calculated from the Kramers−Kronig transform of TRMORD in panel a.

signal-to-noise values compared to TROA are approximately 1:2 and 1:12 for TRMORD and TRORD, respectively.

The millisecond bimolecular recombination processes in both TROA and TRMORD (TRORD) agree in rate and amplitude with other studies on human (*15*−*17*), horse (*44*), and SW Mb (*45*) using TROA spectroscopy in the Soret band. The time constant for the TROA data in Table 1 corresponds to a bimolecular rate constant of 7.9 (±0.3) × 10^5 M^{-1} s^{-1} (26 °C). This agrees well with the value of 7.2 (±0.1) × 10^5 M^{-1} s^{-1} reported for SW Mb (22 °C) by Henry et al. (*46*), for instance, particularly given the differences in species and temperatures. The spectral shapes in absorption and MORD are both consistent with bimolecular recombination. The MORD recombination b-spectrum is more structured than its absorption counterpart, as is apparent from Figures 7 and 10.

DISCUSSION

Geminate and Bimolecular CO Recombination. Previous Soret band TROA experiments on SW myoglobin revealed a 180 ns, 4% amplitude process assigned to geminate recombination on the basis of its CO concentration independence and spectral shape (*46*). Results of TROA spectroscopy in the Soret and near-UV bands of horse myoglobin have also been interpreted in terms of a geminate process with a similar lifetime and amplitude (*44*). The kinetics of this geminate process are clearly nonexponential at temperatures below about 200 K, this kinetic complexity being attributed to the existence of a hierarchy of nonequilibrium conformational substates from which photolysis and geminate rebinding occur (*47*, *48*). Although the relaxation kinetics are expected to become more exponential at higher temperatures, as the interconversions between substates becomes more rapid, previous workers have modeled nonexponential rebinding to room-temperature solution myoglobin with two exponentials or with a stretched exponential (*45*). The kinetic data obtained in this study, however, did not show significant nonexponential character.

The Soret transitions are strongly allowed and relatively insensitive to perturbation by protein conformational relaxation at the heme pocket, so the spectral changes within the first several hundred nanoseconds after Mb−CO photolysis are dominated by the effect of geminate recombination. The visible bands, on the other hand, are weakly allowed, and the absorption and MORD spectral changes associated with τ_1 should have a larger contribution from protein relaxation effects.

Because the spectral signature of the earliest process in this study shows clear differences from that expected for ligand recombination, it most probably involves an intraprotein relaxation after photolysis that is distinct from any heme ligation change, such as geminate recombination. There is precedent for the proposed relaxation process in that small shifts that are consistent with spectral differences associated with conformational change have been observed in geminate recombination Soret spectra (*44*, *46*) in human Mb (*18*) and SW Mb (*49*) in glycerol. The larger spectral signature for protein relaxation seen in this study suggests that structural relaxations rather than geminate ligand recombination to heme may be the dominant contributor to the sub-microsecond visible band spectral evolution of myoglobin. In any event, as this protein relaxation occurs on the time scale expected for geminate recombination, the b-spectrum may actually be a mixture of ligand recombination and protein relaxation contributions. The exact description of this mixture would then depend on the detailed kinetics of geminate ligand escape and entry, information that is not presently available.

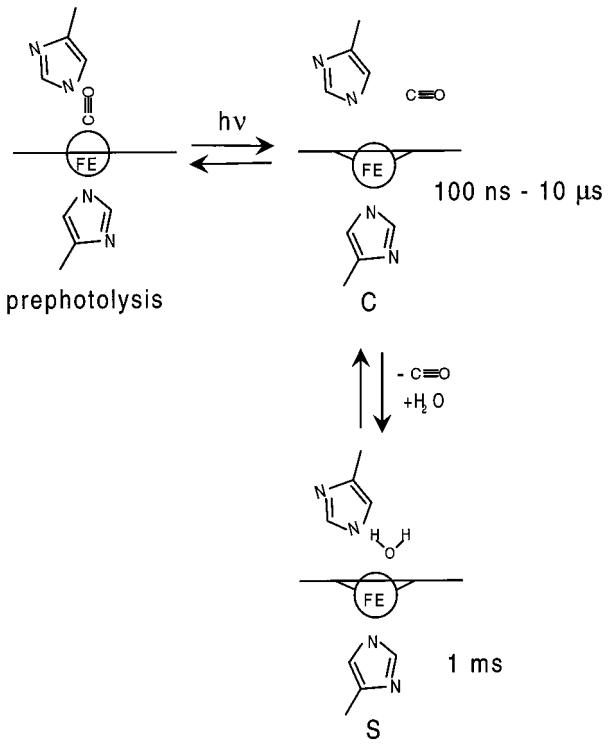

FIGURE 11: Schematic model of MbCO kinetic intermediates and their lifetimes after nanosecond photolysis. In state C, CO is dissociated from the heme but remains in the heme pocket. In state S, CO has migrated into the solvent.

Sub-Microsecond Conformational Changes. Ultrafast transient absorption spectroscopy shows that a deoxy-like absorption spectrum appears within hundreds of femtoseconds following photolysis (*50*). This suggests that most of the heme-localized structural differences between ligated and unligated myoglobin are relaxed on a sub-picosecond time scale. The TROA and TRMORD spectra seen at the earliest nanosecond times presented here also appear to be very much deoxy-like. However, some spectral differences are observed which appear to monitor relaxation of the protein to its equilibrium deoxy state.

These observations are discussed with respect to a preliminary model shown schematically in Figure 11. The prephotolysis Mb has a planar heme with CO bound. Several nanoseconds following ligand photolysis, CO migrates away from the now domed heme into the distal pocket; this is called the C state [sub-nanosecond states are generally referred to as A and B (*7*)]. The escape rate of CO has been measured to be on the order of hundreds of nanoseconds in SW myoglobin (*45*, *46*). After an estimated lifetime of 100 ns to 10 μs for state C (*7*), CO escapes into the solvent and water migrates into the heme pocket and forms a hydrogen bond with His64. It seems plausible that both ligand escape and hydration of the heme promote protein rearrangements within the heme pocket. The sub-microsecond process seen in these absorption and MORD measurements should monitor ligand escape or hydration directly through associated protein

conformational changes. The observed sub-microsecond process is thus discussed below with respect to (1) heme hydration, (2) protein structural changes on the distal side of the heme, and (3) structural changes on the proximal side of the heme.

Hydration of the Distal Pocket. X-ray structures of WT SW deoxyMb reveal a water molecule hydrogen bonded to N_ϵ of His64 that is absent from the heme pocket of the CO complex (*6*). Thus, at some time after the photolysis of MbCO, a water molecule must hydrate the heme pocket. Because this water molecule must be displaced before CO binds, it affects the overall rate constant by changing the equilibrium between CO in the distal pocket and the final binding site (*6*, *10*−*12*). Whether hydration precedes or follows ligand escape, it may play an additional role in preventing heme religation as the CO migrates out of the protein.

The spectral changes for the nanosecond process in visible absorption resemble spectral changes associated with heme hydration. The spectroscopic effects of heme dehydration have been studied in His64-substituted SW deoxyMb (*51*); the visible band absorption spectra of polar (His64Tyr) and apolar (His64Phe, His64Leu, and His64Gly) deoxy mutations lacking a distal water molecule show a 4 nm red shift and broadening in band shape compared with those of the wild type. (These spectral changes are contrary to those expected for the solvent effect associated with decreasing polarity upon water removal, indicating that the interaction between the water molecule and protein is more complicated.) The small (3−6 nm) blue shift seen in process 1 is thus consistent with hydration. Moreover, the loss in intensity of the 560 nm band and the peak broadening around 600 nm that accompany process 1 closely resemble the peak broadening and corresponding peak intensity loss (the oscillator strengths remain nearly constant) seen in the visible band spectra of dehydrated mutants (*51*), although it is not clear if they are affected to the same extent.

Other structural changes in the heme pocket resulting from hydration may also contribute to the observed spectral changes. Because the Leu29Phe mutant does not have the same red shift as the other dehydrated heme mutants, its shift was assigned mainly to iron−heme displacement (*51*). It thus appears that a water near the heme plane can both affect iron−heme displacement and interact electrostatically with the heme and surrounding chromophores to give rise to spectral red shifts at the heme through simultaneous mechanisms. This issue is discussed further below in light of the MORD results, which provide a diagnostic of the heme iron−pyrrole environment.

Distal Heme Pocket Relaxation. Heme pocket rearrangement accompanying ligand escape after photolysis and hydration of the deoxy pocket may give rise to the spectral changes observed in the visible band absorption and MORD. In HMb, X-ray structures show a salt bridge between Lys45 (Arg in SW Mb), Asp60, and a heme propionate (*14*, *17*). It was suggested that this bridge or a similar residue motion could modulate binding to the heme by providing a kinetic barrier to ligand escape and entry (the barrier height being controlled by the protein conformation) (*14*, *16*, *18*). Photoacoustic spectroscopic studies on SW and horse skeletal Mb show a 700 ns restructuring of the protein that culminates in reformation of this bridge (*52*, *53*). To the extent that disruption or formation of a salt bridge near the heme would perturb the local electronic environment of the heme, the visible band TROA and TRMORD data are consistent with such a conformational change.

Time-resolved Soret band absorption using a double-pulse method combined with Raman spectroscopic studies (*45*, *54*) reveals two forms of Mb in equilibrium, the "open" and "closed" forms, with different bimolecular rebinding rates. These forms interconvert with a time constant between 1 and 10 μs and have been assigned to the rotation of the C_α−C_β bond of the distal histidine. Additionally, time-resolved X-ray structures of photolyzed MbCO crystals with nanosecond resolution (*55*) show that His64 rotates toward the iron about 4 ns after photolysis and the CO migrates away from His64 toward the E helix. This residue motion may both inhibit geminate rebinding and be necessary for ligand escape. His64 motion following photolysis may explain the sub-microsecond conformational changes evident in the visible band absorption and MORD.

Proximal Relaxation. Chemical constraints on the proximal side of the heme pocket can greatly modify the reactivity of heme proteins. The R and T quaternary states of hemoglobin differ in ligand affinity by nearly 2 orders of magnitude (*56*), and the geminate recombination observed in the R state disappears in the T state (*57*). The R and T states differ by a relative motion of the dimeric subunits making up the tetramer that tenses the F helix and tilts the proximal histidine−Fe bond relative to the heme plane. The resulting steric interaction between the proximal histidine and porphyrin ring impedes motion of the heme iron into the heme plane, inhibiting the coordination of a sixth ligand (*58*). Soybean leghemoglobin shows a higher affinity for both O_2 and CO than SW Mb. This has been attributed to a greater mobility of the proximal histidine that facilitates in-plane motion of the heme iron and, hence, a higher reactivity to ligation (*59*).

The possible role of dynamical changes in proximal heme geometry in modulating the reactivity of Mb is an open question. It is feasible that after ultrafast doming of the heme, the proximal histidine is not yet completely relaxed to its final, equilibrium position, this relaxation occurring more slowly as the protein chains overcome hydrophobic contact barriers to reach a tertiary conformation that better accommodates the out-of-heme-plane histidine motion. Such a mechanism may play a role in modulating geminate recombination. Spectral changes in the deoxy photoproduct of SW Mb observed in high-viscosity solvent have been interpreted as protein conformational changes on the proximal side of the heme (*49*).

The absorption spectrum of T-state deoxyHb, with a tensed heme, shows that both the main peak at 556 nm and a small shoulder at 510 nm are blue shifted (by about 2 nm) and that a shoulder at 590 nm gains intensity compared with the proximally relaxed R state (*60*). These spectral changes are somewhat similar to the sub-microsecond spectral evolution in Mb observed in this study. This would imply a transition from an "R-like" to a "T-like" state after ligand photolysis. The MORD of deoxyHb is particularly sensitive to tertiary structure changes at the heme that accompany a change in the quaternary state. There is a >50% increase in the magnitude of the 585 nm band for the T state compared with R state (*61*, *62*). The presence in Mb of an out-of-heme iron

displacement and proximal histidine motion paralleling that seen in Hb should thus have a pronounced effect on the MORD. However, the sub-microsecond TRMORD spectral evolution observed in photolyzed horse Mb is smaller with respect to the changes seen in TROA than would be expected on this basis, and a proximal relaxation similar to that in Hb is not indicated in Mb. Any similar conformational change that directly affects the heme, in particular those associated with lengthening or shortening of the pyrrole nitrogen−iron or histidine−iron bond, is also unlikely because they would again have relatively large effects on the MORD data that are not observed.

In conclusion, the visible band TRMORD and TROA data show a sub-microsecond protein relaxation after CO photolysis, but the MORD data do not support a major role for iron−histidine or iron−pyrrole bond relaxation on the proximal side of the heme in explaining the associated spectral changes. On the basis of the comparison of the MORD spectral changes observed here with those associated with the relaxation of proximal histidine geometry in Hb, the Mb spectral changes are found to be more consistent with a conformational change on the distal side of the heme pocket. In particular, this distal relaxation may be associated with protein residue accommodation to ligand escape, salt bridge rearrangements, or heme hydration. The similarity of the visible band spectral changes observed as the protein relaxes to its deoxy state with those expected for hydration of the heme pocket suggests that the protein relaxation that can be detected in both the visible band absorption and MORD results most probably correlates with heme pocket hydration. This assignment for the fast relaxation process observed in the visible bands can be tested by measuring the spectrokinetics after CO photolysis from Mb mutants lacking a water in the heme pocket, as these are predicted not to show the sub-microsecond relaxation observed here.

ACKNOWLEDGMENT

We thank Drs. James Lewis for technical assistance, Eefei Chen for myoglobin preparation assistance, and Istvan Szundi for valuable discussions about kinetics and global analysis.

REFERENCES

1. Quillin, M. L., Li, T., Olson, J., Phillips, G. N., Dou, Y., Ikeda-Saito, M., Regan, R., Carlson, M., Gibson, Q. H., Li, H., and Elber, R. (1995) *J. Mol. Biol. 245*, 416−436.
2. Olson, J. S., and Phillips, G. N. (1997) *J. Biol. Inorg. Chem. 2*, 544−552.
3. Stryer, L. (1995) *Biochemistry*, Freeman, New York.
4. Verma, A., Hirsch, D. J., Glatt, C. E., Ronnett, G. V., and Snyder, S. H. (1993) *Science 259*, 381−384.
5. Morita, T., Perrella, M. A., Lee, M. E., and Kourembanas, S. (1995) *Proc. Natl. Acad. Sci. U.S.A. 92*, 1475−1479.
6. Springer, B. A., Sligar, S. G., Olson, J. S., and Phillips, G. N. (1994) *Chem. Rev. 94*, 699−714.
7. Olson, J. S., and Phillips, G. N. (1996) *J. Biol. Chem. 271*, 17593−17596.
8. Collman, J. P., Brauman, J. I., Iveson, B. L., Sessler, J. L., Morris, R. M., and Gibson, Q. M. (1983) *J. Am. Chem. Soc. 105*, 3052−3064.
9. Springer, B. A., Egeberg, K. D., Sligar, S. G., Rohlfs, R. J., Mathews, A. J., and Olson, J. S. (1989) *J. Biol. Chem. 264*, 3057−3060.
10. Gibson, Q. H., Olson, J. S., McKinnie, R. E., and Rohlfs, R. J. (1986) *J. Biol. Chem. 261*, 10228−10239.
11. Jongeward, K. A., Madge, D., Taube, D. J., Marsters, J. C., Traylor, T. G., and Sharmam, V. S. (1988) *J. Am. Chem. Soc. 110*, 3380−3387.
12. Carver, T. E., Rohlfs, R. J., Olson, J. S., Gibson, Q. H., Blackmore, R. S., Springer, B. A., and Sligar, S. G. (1990) *J. Biol. Chem. 265*, 20007−20020.
13. Nobbs, C. L. (1966) in *Hemes and Hemeproteins* (Chance, B., Eastbrook, R. W., and Yonetani, T., Eds.) pp 143−147, Academic Press, New York.
14. Lambright, D. G., Balasubramanian, S., and Boxer, S. G. (1991) *Chem. Phys. 158*, 249−260.
15. Balasubramanian, S., Lambright, D. G., Simmons, J. H., Gill, S. J., and Boxer, S. G. (1994) *Biochemistry 33*, 8355−8360.
16. Lambright, D. G., Balasubramanian, S., Decatur, S. M., and Boxer, S. G. (1994) *Biochemistry 33*, 5518−5525.
17. Balasubramanian, S., Lambright, D. G., Marden, M. C., and Boxer, S. G. (1993) *Biochemistry 32*, 2202−2212.
18. Lambright, D. G., Balasubramanian, S., and Boxer, S. G. (1993) *Biochemistry 32*, 10116−10124.
19. Goutermann, M. (1978) in *The Porphyrins* (Dolphin, D., Ed.) Vol. III, pp 1−165, Academic Press, New York.
20. Adar, F. (1978) in *The Porphyrins* (Dolphin, D., Ed.) Vol. III, pp 167−209, Academic Press, New York.
21. Weiss, C., Kobayashi, H., and Goutermann, M. (1965) *J. Mol. Spectrosc. 16*, 415−428.
22. Perrin, M. H., Goutermann, M., and Perrin, C. L. (1969) *J. Chem. Phys. 50*, 4137−4147.
23. Eaton, W. A., and Hofrichter, J. (1981) *Methods Enzymol. 76*, 175−261.
24. Dawson, J. H., and Dooley, D. M. (1989) in *Iron Porphyrins, Part 3* (Lever, A. B. P., and Gray, H. B., Eds.) pp 1−135, VCH, New York.
25. Shashoua, V. E. (1973) *Methods Enzymol. 27*, 796−810.
26. Cheesman, M. R., Greenwood, C., and Thomson, A. J. (1991) *Adv. Inorg. Chem. 36*, 201−255.
27. Moscowitz, A. (1962) *Adv. Chem. Phys. 4*, 67−112.
28. Barron, L. D. (1982) *Molecular Light Scattering and Optical Activity*, Cambridge University Press, Cambridge, U.K.
29. Jackson, J. D. (1975) *Classical Electrodynamics*, Wiley, New York.
30. Shapiro, D. B., Goldbeck, R. A., Che, D., Esquerra, R. M., Paquette, S. J., and Kliger, D. S. (1995) *Biophys. J. 68*, 326−334.
31. Tinoco, I. (1970) *Methods Biochem. Anal. 18*, 81−203.
32. Johnson, W. C. (1990) *Proteins: Struct., Funct., Genet. 7*, 205−214.
33. Solomon, E. I., Pavel, E. G., Loeb, K. E., and Campochiaro, C. (1995) *Coord. Chem. Rev. 4*, 369−460.
34. Esquerra, R. M., Goldbeck, R. A., Kim-Shapiro, D. B., and Kliger, D. S. (1998) *J. Phys. Chem. 102*, 8740−8748.
35. Esquerra, R. M., Goldbeck, R. A., Kim-Shapiro, D. B., and Kliger, D. S. (1998) *J. Phys. Chem. 102*, 8749−8758.
36. Keston, A., and Lospalluto, J. (1953) *Fed. Proc. 12*, 229.
37. Esquerra, R. M. (1997) Ph.D. Dissertation, University of California, Santa Cruz, CA.
38. Kliger, D. S., and Lewis, J. W. (1987) *Rev. Chem. Intermed. 8*, 367−398.
39. Lewis, J. W., Tilton, R. F., Einterz, C. M., Milder, S. J., Kuntz, I. D., and Kliger, D. S. (1985) *J. Phys. Chem. 89*, 289−294.
40. Golub, G. H., and Reinsch, C. (1970) *Numerische Mathematik 14*, 403−420.
41. Henry, E. R., and Hofrichter, J. (1991) *Methods Enzymol. 210*, 129−192.
42. Goldbeck, R. A., Paquette, S. J., Björling, S. C., and Kliger, D. S. (1996) *Biochemistry 35*, 8628−8639.
43. Goldbeck, R. A., and Kliger, D. S. (1993) *Methods Enzymol. 226*, 147−177.
44. Chen, E., and Kliger, D. S. (1996) *Inorg. Chim. Acta 242*, 146−158.
45. Tian, W. D., Sage, J. T., Šrajer, V., and Champion, P. M. (1992) *Phys. Rev. Lett. 68*, 408−411.
46. Henry, E. R., Sommer, J. H., Hofrichter, J., and Eaton, W. A. (1983) *J. Mol. Biol. 166*, 443−451.

47. Austin, R. H., Beeson, K. W., Eisenstein, L., Frauenfelder, H., and Gunsalus, I. C. (1975) *Biochemistry 14*, 5355−5373.
48. Ansari, A., Berendzen, J., Bowne, S. F., Frauenfelder, H., Iben, I. E. T., Sauke, T. B., Shyamsunder, E., and Young, R. D. (1985) *Proc. Natl. Acad. Sci. U.S.A. 82*, 5000−5004.
49. Ansari, A., Jones, C. M., Henry, E. R., Hofrichter, J., and Eaton, W. A. (1992) *Science 256*, 1796−1798.
50. Martin, J. L., Migus, A., Poyart, C., Lecarpentier, Y., Astier, R., and Antonetti, A. (1983) *Proc. Natl. Acad. Sci. U.S.A. 80*, 173−177.
51. Christian, J. F., Unno, M., Sage, J. T., Champion, P. M., Chien, E., and Sligar, S. G. (1997) *Biochemistry 36*, 11198−11204.
52. Westrick, J. A., and Peters, K. S. (1990) *Biophys. Chem. 37*, 73−79.
53. Westrick, J. A., Goodman, J. L., and Peters, K. S. (1987) *Biochemistry 26*, 8313−8318.
54. Tian, W. D., Sage, J. T., and Champion, P. M. (1993) *J. Mol. Biol. 233*, 155−166.
55. Šrajer, V., Teng, T. Y., Ursby, T., Pradervand, C., Ren, Z., Adachi, S., Schildkamp, W., Bourgeois, D., Wulff, M., and Moffat, K. (1996) *Science 274*, 1726−1729.
56. Parkhust, L. J. (1979) *Annu. Rev. Phys. Chem. 30*, 503−546.
57. Murray, L. P., Hofrichter, J., Henry, E. R., Ikeda-Saito, M., Kitagishi, K., Yonetani, T., and Eaton, W. A. (1988) *Proc. Natl. Acad. Sci. U.S.A. 85*, 2151−2155.
58. Perutz, M. F. (1990) *Annu. Rev. Phys. 52*, 1−25.
59. Harutyunyan, E. H., Safonova, T. N., Kuranova, I. P., Popov, A. N., Teplyakov, A. V., Obmolova, G. V., Rusakov, A. A., Vainshtein, B. K., Dodson, G. G., Wilson, J. C., and Perutz, M. F. (1995) *J. Mol. Biol. 251*, 104−115.
60. Perutz, M. F., Ladner, J. E., Simon, S. R., and Ho, C. (1974) *Biochemistry 13*, 2163−2173.
61. Sharonov, Y., and Sharonova, N. A. (1976) *Biochim. Biophys. Acta 446*, 547−553.
62. Sharonov, Y. A., Sharonova, N. A., and Atanasov, B. P. (1976) *Biochim. Biophys. Acta 434*, 440−451.
63. Quillin, M. L., Arduini, R. M., Olson, J., and Phillips, G. N. (1993) *J. Mol. Biol. 234*, 140−155.

BI9814437